Spin polarization and many-body effects in Ni 3*p* core-level photoemission

J. G. Menchero
Department of Physics, University of California at Berkeley, Berkeley, California 94720
and Materials Sciences Division, Lawrence Berkeley Laboratory, University of California, Berkeley, California 94720
(Received 9 January 1997; revised manuscript received 2 September 1997)

Photoemission spectra are calculated for the Ni 3*p* core level within a small-cluster many-body scheme, and compared to experimental results. The effects of spin-orbit coupling, electron-electron interaction, and extra-atomic screening are understood by examining theoretical spectra for a variety of limiting cases. The transfer of spectral weight between the satellites and the main lines is found to depend on the ratio of the valence bandwidth to the effective Hubbard interaction U_{eff}. Local final-state configurations are reported, and a physical interpretation of the various spectral peaks is given. [S0163-1829(98)07501-8]

I. INTRODUCTION

In a typical core-level photoemission experiment, monochromatic light of wave vector **q**, polarization ϵ, and energy $\hbar\omega$ impinges on a sample, exciting the core electrons into free electron states far above the Fermi sea. The wave vector **k**, kinetic energy E_k, and perhaps also the spin σ of these photoelectrons are then measured. Knowing E_k and $\hbar\omega$ allows one to deduce the electron binding energy E_B via the simple relation: $E_B=\hbar\omega-E_k$. The core-level binding energies of the elements are well known, and so a peak in a photoemission spectrum at a certain binding energy serves as a sort of ''atomic fingerprint'' for the presence of a given species of atom. This makes core-level photoelectron spectroscopy a powerful element-specific probe of condensed-matter systems.

The itinerant ferromagnets Fe, Co, and Ni are particularly interesting systems to investigate via photoelectron spectroscopy. In these systems, the core electrons are coupled to the spin-polarized valence electrons through the Coulomb and exchange interactions. Therefore, core electrons with spin parallel to the majority in the valence band should see their average position shifted to higher binding energy. In spin-resolved x-ray photoelectron spectroscopy (SRXPS), the spin of the outgoing photoelectron is also measured, and these spin-polarized spectra therefore serve as a direct probe of the local electronic and magnetic environment. Such SRXPS studies have by now been carried out for both the shallow[1,2] as well as the deep[3–5] core levels of the itinerant ferromagnets.

For the relatively delocalized transition metals Fe and Co, one-electron theories[6,7] reproduce experimental results relatively well for 2*p* and 3*p* core levels. This single-particle approach clearly breaks down for a localized atomiclike system, where coupling between the core hole and the valence shell results in a complex multiplet structure. For such systems, the spectra cannot be described by considering only six lines.

For Ni, the situation is complicated by the fact that it not only exhibits a multiplet structure, but also displays extra-atomic screening effects. Therefore, both the *localized* and the *delocalized* properties of the valence electrons are manifest in the photoemission spectrum. It is this ''intermediate coupling'' nature of Ni that makes it a particularly fascinating system to study.

Up to now, most theoretical efforts to describe core-level photoemission from Ni have been based on an Anderson impurity model.[2,8] In this model, Ni is treated as an ''impurity'' within a Ni host, and extra-atomic screening is described in terms of hybridization of valence orbitals with adjacent atoms through an adjustable ''mixing parameter.''

An alternative approach is the periodic small-cluster model used by Victora and Falicov[9] to describe the Ni valence-band photoemission spectrum, and by Menchero[10,11] for the Ni 2*p* core level. It is this model which we extend here to consider the case of photoemission from the Ni 3*p* core level. Unlike the Anderson model, this model contains translational symmetry due to periodicity. Translational symmetry implies a band structure, which in turn describes the hopping of the valence electrons. Therefore, extra-atomic screening in this model is treated naturally by way of the electronic band structure.

This paper is organized as follows: In Sec. II we provide a brief description of the model. We then present the calculated Ni 3*p* spin-resolved spectra and make a detailed comparison to experimental results. In Sec. III we present and discuss spin-resolved spectra for a variety of limiting cases. This analysis provides important insights into the underlying physics. We also present results from a simple model that correctly explains the transfer of spectral weight between the satellites and the main lines. We then discuss hybridization effects between d^8, d^9, and d^{10} configurations, and plot the local atomic configuration as a function of binding energy. Conclusions are given in Sec. IV.

II. RESULTS

Our model has been described elsewhere.[11] Briefly, it consists of a tetrahedral cluster of four Ni atoms, with periodic boundary conditions imposed to generate the full fcc lattice. Each atom in the lattice can be labeled by an index 1–4, and is surrounded by 12 nearest neighbors of a different index. Such periodicity dictates that all Bloch states must transform according to either Γ or X in the Brillouin zone.

Our Hamiltonian contains three types of terms: core-level spin-orbit coupling, intrasite electron-electron Coulomb re-

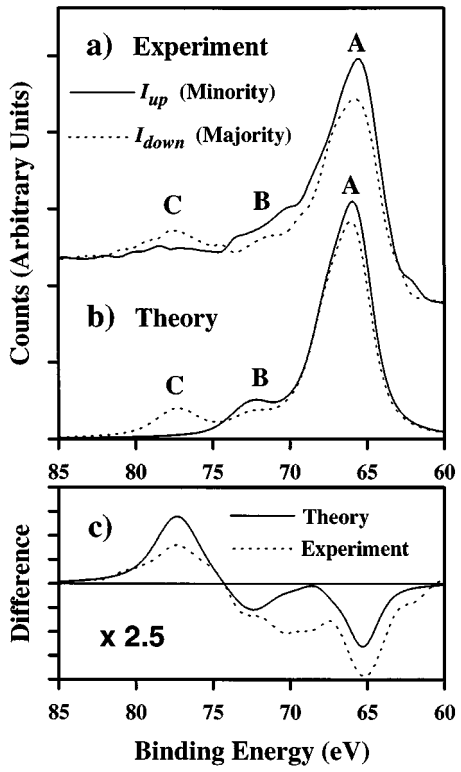

FIG. 1. Experimental and theoretical SRXPS results. (a) Experimental results taken at $\hbar\omega = 1253.6$ eV. (b) Theoretical results. Lines were convoluted with Gaussian (FWHM=1.6 eV) and Lorentzian (1.5 eV FWHM at A and B, 2.5 eV at C) line shapes to simulate instrumental and lifetime broadenings. (c) Theoretical and experimental spin polarizations, multiplied by 2.5 for clarity.

pulsion, and valence-band hopping. For the spin-orbit splitting between the $j=3/2$ and $j=1/2$ core levels we use 1.74 eV, a value used by previous workers.[2] The Coulomb interaction is described in terms of the standard Slater integrals, and we again adopt the values of previous workers.[2] The valence-band hopping is described by means of the electronic band structure. We match the energies of the Bloch states at Γ and X in our model to the spin-averaged band-structure calculations of Wang and Callaway.[12]

The ground state in our model is ferromagnetic with a 50% d^9 and 50% d^{10} initial-state configuration, leading to a spin moment of $0.50\mu_B$ per atom. In this work, we use the sign convention that the magnetization direction is ''up,'' meaning that the majority electrons are spin *down*. Spectra are calculated using Fermi's golden rule within the electric dipole approximation. We include interference between the $l\pm1$ channels, and use the channel matrix elements and phase shifts of Goldberg, Fadley, and Kono.[13] Photoelectron diffraction effects are not considered in this work.

In Fig. 1(a) we present experimental Ni $3p$ spin-resolved spectra due to See and Klebanoff.[5] A single-crystal Ni sample, remanently magnetized in the surface plane, was irradiated with a Mg $K\alpha$ x-ray source. Photoelectrons were collected normal to the surface and their spin measured along the magnetization direction. Instrumental resolution was estimated at 1.6 eV full width at half maximum (FWHM). Solid (dashed) lines are for photoelectrons with spin parallel to the minority (majority) electrons in the valence band. The experimental results are characterized by three main features: a broad main line (labeled A), and two satellite structures (labeled B and C) centered about $\sim$72 and $\sim$77 eV. The main line displays a strong minority-spin polarization, as does satellite B. Satellite C, on the other hand, exhibits a strong majority-spin polarization.

In Fig. 1(b) we present the corresponding theoretical spin-resolved spectra, which were calculated for normal emission and a grazing-angle geometry, i.e., photon **q** was taken parallel to magnetization **M**, with photoelectron **k** normal to **M**. We use channel matrix elements taken at Mg $K\alpha$ photon energy.[13] Lines were convoluted with a Gaussian (1.6 eV FWHM) to simulate instrumental broadening, and by Lorentzians (1.5 eV FWHM for A and B, 2.5 eV for C) to simulate lifetime broadening. For narrower broadenings, the well-known 2-eV shoulder emerges in the main line. For the relatively wide broadenings used here, however, this shoulder is hardly discernible.

The theoretical results correctly reproduce all the principal features of the experimental spectra. Furthermore, the relative positions and intensities of peaks A, B, and C agree very well with observations.

In Fig. 1(c) we plot the theoretical and experimental spin polarizations. In both theory and experiment, feature C has a strong majority-spin polarization, whereas features A and B exhibit minority-spin polarizations. While the theoretical results correctly predict the *sign* of the spin polarization throughout the spectrum, the *magnitude* is overestimated at C and underestimated at A and B. This could be due to a net minority background spin polarization within this energy range. Since the core is fully occupied in the initial state, the spin polarization integrated over the energy range of the core shell should vanish:

$$\int_{\text{core}} (I_{\text{up}} - I_{\text{down}})\,dE = 0. \tag{1}$$

It is apparent that the experimental spectra do not satisfy this condition. Agreement between theory and experiment would be clearly improved by removing such a background.

III. DISCUSSION

The Ni $3p$ spectrum exhibits several complex subtleties due to the interplay between Coulomb and exchange interaction, spin-orbit coupling, and extra-atomic screening. In order to gain physical insight into the underlying structure, we consider here a variety of limiting cases. From Fig. 1, we see that the satellites are spread over a manifold of more than 12 eV. Spin-orbit splitting, on the other hand, is only 1.74 eV. This suggests that LS coupling is a reasonably good starting point for describing the satellite structures. We then discuss the transfer of spectral weight between satellites and main lines, and show that the effect can be understood in terms of a simple 2×2 model. Finally, we turn to the question of final-state configurations. This allows us to describe in a more quantitative way the physical nature of the final states.

A. Spin polarization

In this section we present theoretical spin-resolved spectra for a variety of limiting cases, with the same grazing-angle

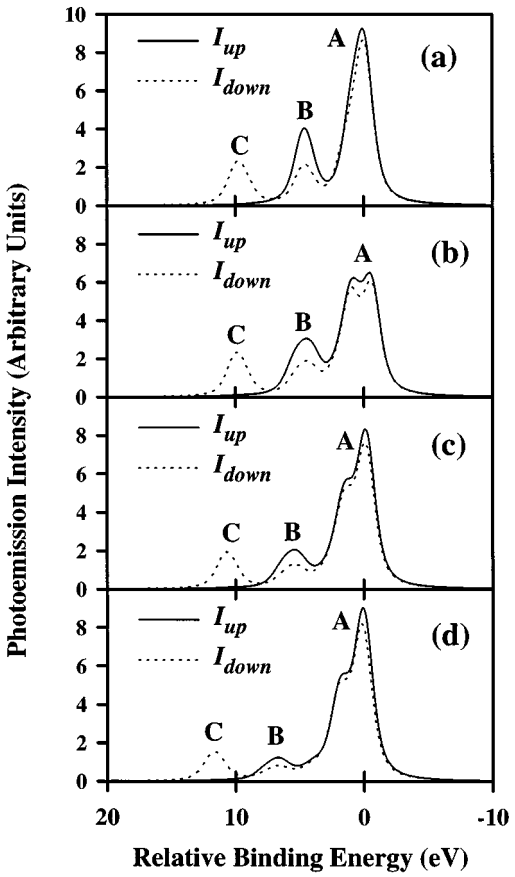

FIG. 2. Theoretical spin-polarized photoemission spectra, with spin-up (down) corresponding to minority (majority) photoelectrons. All lines were broadened with Gaussian (FWHM=1 eV) and Lorentzian (FWHM=1 eV) line shapes. (a) SRXPS for zero core-level spin-orbit splitting, and zero valence bandwidth. (b) SRXPS for $3p$ spin-orbit splitting of 1.74 eV, and zero valence bandwidth. (c) and (d) SRXPS for 1.74 eV spin-orbit splitting, with 50% and 100% valence bandwidth, respectively.

geometry described in Sec. II. Lines were convoluted with Gaussian (FWHM=1 eV) and Lorentzian (FWHM=1 eV) line shapes and the channel matrix elements were taken at 400-eV photon energy.[13]

As our first case, we consider the spin-resolved spectra in the limit of LS coupling and zero valence bandwidth. We obtain the zero-bandwidth limit by setting the energies of all the Bloch states to zero. For this case, because there is no hopping, the number of valence electrons on the core-hole atom in the final state is a good quantum number. In this way, each line in the spectrum can be assigned a precise physical interpretation. We obtain the LS limit by setting the spin-orbit coupling to zero. In this case, the total L and total S of the core-hole atom are good quantum numbers.

The spin-resolved spectra are presented in Fig. 2(a). As before, majority electrons are spin down. Even in this limit, already the gross features of the actual Ni $3p$ spectra are apparent: i.e., a main line A and two satellites B and C, each with the correct spin polarization. The most obvious discrepancies between these spectra and the actual SRXPS spectra are that the satellite intensities are too large and that there is no 2-eV shoulder in the main line.

For this simple limit, it is instructive to examine in greater detail the underlying structure of the spectra. If the core hole is created at a site that is locally d^9, then the core hole and the valence hole angular momenta couple according to the LS scheme. The resulting terms, in order of increasing binding energy, are: ^3F, ^1D, ^3P, ^3D, ^1P, and ^1F.

The spectrum in this limit therefore contains exactly seven lines: a single d^{10} line and six lines for the d^9 configuration. The leading edge of the main line is found to be d^{10}, with the ^3F and ^1D lines being $\sim 1-2$ eV higher in binding energy. Structure B is due to the ^3P and ^3D terms, and structure C is due to ^1P and ^1F. The spin-resolved intensities of these lines obey the following properties:

(a) The d^{10} line, being intrinsically nonmagnetic, is unpolarized.

(b) The net intensities of the d^9 and d^{10} lines are in exact proportion to their ground-state populations; i.e., 50% of the line strength is d^9 and 50% d^{10}.

(c) The d^9 triplet lines are minority-spin polarized in the ratio 2:1; the singlet lines are 100% majority-spin polarized.

(d) The spin-integrated strengths of the d^9 lines are proportional to the number of states in the terms: e.g., $I(^3P)/I(^1P)=3:1$, $I(^3D)/I(^3P)=5:3$, etc.

Therefore, in this limit, the leading edge of the main line is d^{10}, but the spin polarization is due to the ^3F term. Feature B, composed of triplet lines, is strongly minority-spin polarized, whereas feature C is due to singlets and is therefore 100% majority-spin polarized.

As our next case, we introduce a realistic spin-orbit splitting of 1.74 eV between $p_{3/2}$ and $p_{1/2}$, but maintain the valence bandwidth at zero. With nonzero spin-orbit coupling, total L and total S of the core-hole atom are no longer strictly good quantum numbers. Total angular momentum J of the core-hole atom is still rigorously a good quantum number, and the triplet terms break up into individual lines of definite J. Therefore, in this limit, the spectrum consists of 14 lines: the spin-orbit split d^{10} lines and the 12 d^9 lines.

The spin-resolved spectra for this case are presented in Fig. 2(b). Satellite C is almost unchanged from the strict LS limit case. However, satellite B is noticeably broader due to the splitting of the ^3P and ^3D terms. The most obvious change with the introduction of spin-orbit coupling is the appearance of a ''twin peak'' structure in the main line.

Again, since the number of lines is so limited, and because each line can be unambiguously assigned, it is instructive to examine in greater detail the intensities of the lines. We note the following observations:

(a) The d^{10} lines are unpolarized. The d^{10} lines are intrinsically nonmagnetic and so can exhibit no exchange-induced spin polarization. Although there can be spin-orbit-induced spin polarization in a d^{10} line,[14] in the nonchiral geometry considered here such effects are not present. Therefore, the spin polarization is determined exclusively by the d^9 configuration.

(b) The relative intensities of the $p_{3/2}d^{10}$ to $p_{1/2}d^{10}$ lines is 2:1, a reflection of the $2j+1$ multiplicity of the levels.

(c) The relative spin-integrated intensities of the d^9 lines are proportional to the multiplicity $2J+1$.

(d) The spin polarization of the $^1D_2$ line is effectively neutralized through strong mixing with the $^3F_2$ line. This

example clearly demonstrates the strong hybridization effects that occur when two energetically nearby lines are allowed to mix. Before spin-orbit coupling is turned on, the ^1D line is 100% spin down, and energetically separated by only ~ 0.5 eV from the ^3F line, which is primarily spin up. With spin-orbit coupling, the lines repel and $^1D_2$ acquires much of the spin-up character of $^3F_2$, and vice versa.

(e) The main-line leading edge is $p_{3/2}d^{10}$ and the high-binding-energy ''twin peak'' is due to ^3F and $p_{1/2}d^{10}$.

Next we consider the effect of extra-atomic screening by introducing a narrow valence bandwidth. This is accomplished by multiplying the energies of the Bloch states of Wang and Callaway[12] by a scaling factor of 0.50. The resulting spectra are presented in Fig. 2(c). With a small but nonzero bandwidth, configurations can mix, meaning that the electron occupancy of the core-hole atom is no longer a good quantum number. Also, line strength is now transferred from the high-binding-energy side of the spectrum to the low-binding-energy side, i.e., satellites *B* and *C* lose intensity to the main line. This is also true *within* the main line: the high-binding-energy ''twin'' in the main line transfers intensity to the low-binding-energy side, and thereby reduces itself to a shoulder.

Although satellite peaks *B* and *C* are no longer pure d^9 due to hybridization, the peaks are still clearly identifiable. In this sense it is still meaningful to assign satellite C to ^1P and ^1F terms, and satellite *B* to ^3P and ^3D terms.

Caution must be exercised in assigning the main line. Before the valence bandwidth is turned on, we find that the $^3F_2$, $^3F_3$, and $p_{1/2}$ lines are energetically separated by only 120 meV. Any mixing between these lines will lead to very strong hybridization, as discussed previously. Therefore, although the Ni 3*p* main line cannot be unambiguously defined, we can say that it consists of a heavily hybridized mixture of $p_{1/2}d^{10}$, ^3F, and $p_{3/2}d^{10}$ lines.

As our final case, we set the valence-band energies equal to their full value as calculated by Wang and Callaway.[12] The resulting spectra are presented in Fig. 2(d). As the bandwidth is increased, extra-atomic screening transfers additional spectral weight from the d^9 satellites to the main line. While satellites *B* and *C* both lose intensity, careful examination of Figs. 2(b)–2(d) show that as the bandwidth is increased from 0 to 100%, satellite *B* loses a *greater* proportion of its intensity. This transfer of spectral weight, which depends sensitively on relative binding energy, is discussed in greater detail below.

We observe further that as the bandwidth is increased, the positions of satellites *B* and *C* are shifted to higher binding energy. This is because a local d^9 excitation, when viewed in *k* space, must contain sizable components of Bloch states from below the Fermi level. As the bandwidth is increased, the energetic cost of promoting these electrons is also increased, and the line shifts to higher binding energy.

Finally, we observe that line strength continues to be transferred within the main line from the high-binding-energy side to the low side. In doing so, the 2-eV shoulder becomes less pronounced.

B. Transfer of spectral weight

In this section we investigate in greater detail how extra-atomic screening transfers spectral weight between a d^9 satellite and a d^{10} main line. In particular, we wish to determine how this transfer depends on the valence bandwidth and satellite position.

From Fig. 2 we see that each satellite maintains its relative spin polarization as intensity is transferred to the main line, although satellites *B* and *C* do not transfer intensity in the same proportion. In other words, to first order, the transfer of spectral weight does not depend on spin, but rather on relative binding energy. This suggests that we can neglect electron spin when modeling the effect.

We choose as our simple model a two-atom system with periodic boundary conditions and one valence orbital per site. In our initial state we have one hole in the valence band, so that the local occupancy fluctuates between zero and one holes. This is in direct analogy to the case of Ni, where the dominant d^{10} and d^9 configurations also lead to local fluctuations of zero or one holes. For spinless electrons, the basis states are given by

$$|f_1\rangle = c^\dagger_{v_1}|0\rangle \tag{2a}$$

$$|f_2\rangle = c^\dagger_{v_2}|0\rangle, \tag{2b}$$

where $c^\dagger_{v_i}$ creates a valence hole at site i. If t is the hopping parameter for holes, then the Hamiltonian matrix is given by

$$H = \begin{bmatrix} 0 & t \\ t & 0 \end{bmatrix}. \tag{3}$$

The ground state has energy $-t$ and is given by

$$|GS\rangle = \frac{|f_1\rangle - |f_2\rangle}{\sqrt{2}}. \tag{4}$$

The antibonding state is at energy $+t$ and hence the valence bandwidth is $BW = 2t$. Upon photoemission, a core hole is created, and our new basis states become

$$|g_1\rangle = c^\dagger_{c_1}|f_1\rangle, \tag{5a}$$

$$|g_2\rangle = c^\dagger_{c_1}|f_2\rangle, \tag{5b}$$

where $c^\dagger_{c_1}$ creates a core hole at site 1. The Hamiltonian H' after photoemission is given by

$$H' = \begin{bmatrix} U & t \\ t & 0 \end{bmatrix}, \tag{6}$$

where U is the Hubbard term which describes the intrasite Coulomb repulsion between the core hole and the valence hole. The (un-normalized) eigenstates of H' are

$$|e^+\rangle = (U + \sqrt{U^2 + 4t^2})|g_1\rangle + 2t|g_2\rangle, \tag{7a}$$

$$|e^-\rangle = 2t|g_1\rangle - (U + \sqrt{U^2 + 4t^2})|g_2\rangle. \tag{7b}$$

In the limit $t \to 0$, we see $|e^+\rangle \sim |g_1\rangle$ and $|e^-\rangle \sim |g_2\rangle$. In other words, $|e^+\rangle$ corresponds to the satellite and $|e^-\rangle$ to the main line. We obtain the satellite intensity in the sudden approximation by projection

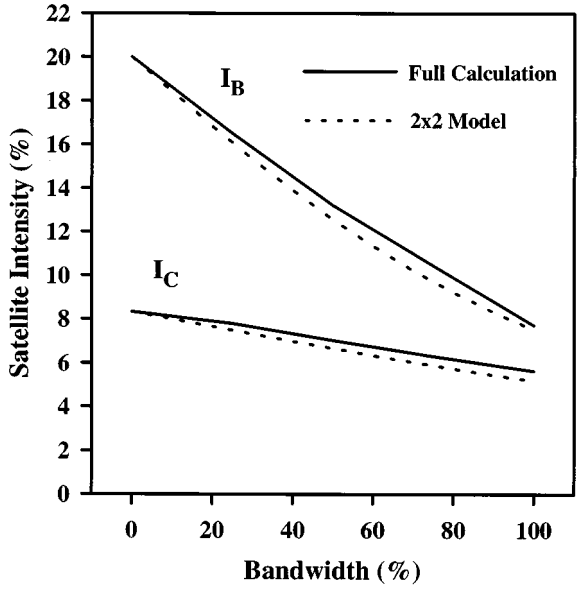

FIG. 3. Spin-integrated intensities of satellites B and C as a function of valence bandwidth, for unpolarized excitation. Satellite intensities are given as a percent of total Ni $3p$ line strength. The solid lines are the result of an exact numerical integration using the full many-body eigenstates. The dashed lines are the results of a simple 2×2 model described in the text, using (at 100% bandwidth) $\tau=0.80$ for satellite B and $\tau=0.41$ for satellite C.

$$I_{\rm sat}=\frac{|\langle e^+|c_{c_1}^\dagger|GS\rangle|^2}{\langle e^+|e^+\rangle}. \tag{8}$$

If we define the dimensionless parameter $\tau=BW/U$, then the result is given by

$$I_{\rm sat}=I_0\left[\frac{1-\tau+\tau^2+(1-\tau)\sqrt{1+\tau^2}}{1+\tau^2+\sqrt{1+\tau^2}}\right], \tag{9}$$

where I_0 is the satellite intensity in the limit of zero valence bandwidth (in this example, $I_0=0.5$). In the narrow bandwidth limit, Eq. (9) reduces to $I_{\rm sat}=I_0(1-\tau)$; i.e., the satellite intensity is predicted to decrease linearly with increasing valence bandwidth.

To study how well Eq. (9) describes the screening process in Ni, we must first determine $\tau=BW/U$ for the satellites. The Ni valence bandwidth is 4.31 eV.[12] For U, we must use the *effective* Hubbard interaction $U_{\rm eff}$, defined here as the energy separation in the limit of zero valence bandwidth between the satellite and the leading edge of the main line. This is roughly 5.4 eV for satellite B and roughly 10.4 eV for satellite C. Hence, for full valence bandwidth, we have $\tau_B=0.80$ and $\tau_C=0.41$. In Fig. 3 we plot the intensities of satellites B and C as a function of valence bandwidth. These intensities were calculated two different ways: first by means of numerical integration using the full many-body calculation and second by using Eq. (9). The two approaches yield results that are in excellent agreement, indicating that the important quantity governing the transfer of spectral weight is the ratio of the valence bandwidth to the effective Hubbard repulsion.

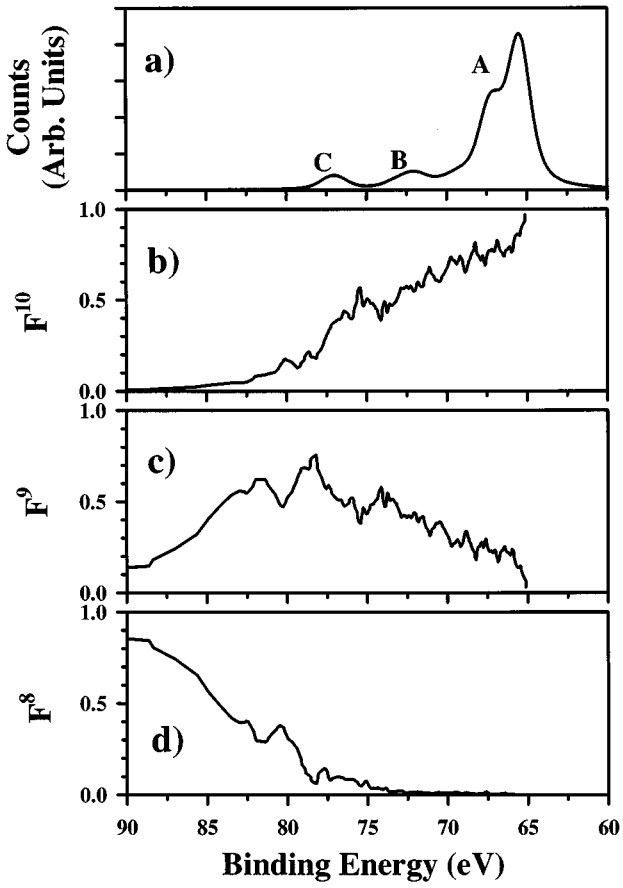

FIG. 4. Local final-state configuration. (a) Ni $3p$ spin-integrated results for unpolarized excitation. (b)–(d) Fraction of d^{10}, d^9, and d^8 local final-state configuration as a function of binding energy.

C. Final-state configuration

In this section we examine in greater detail hybridization effects and the nature of the final state. Upon photoexcitation, a localized core hole is created at a particular site, leading to a sudden attractive potential for nearby electrons. If the core hole is created at a site that is locally d^9, then an electron from a neighboring atom can hop into the unoccupied valence orbital, thereby screening the core hole. This extra-atomic screening leads to mixing of the configurations.

For a given final eigenstate $|\Psi_f\rangle$, of energy E_f, we wish to know the local number of valence electrons on the core-hole atom. Let $|d_k^n\rangle$ be the kth basis state with exactly n valence electrons on the photoexcited atom. We then calculate the local atomic configuration according to

$$F^n(E_f)=\sum_k |\langle d_k^n|\Psi_f\rangle|^2, \tag{10}$$

where $F^n(E_f)$ gives the fractional probability of finding the final eigenstate of energy E_f with n valence electrons on the core-hole atom. We then average over a sufficiently small energy interval to obtain a smooth function over the energy range of core level. Since the valence configuration fluctuates between 8, 9, and 10 electrons,

$$F^8+F^9+F^{10}=1.0 \tag{11}$$

must hold for every eigenstate $|\Psi_f\rangle$.

In principle, such a description could be misleading. Consider the zero bandwidth limit. In this case, each line in the spectrum can be unambiguously assigned to either d^9 or d^{10} configurations, e.g., the satellites are pure d^9 final states. However, there may be d^{10} states (*of zero intensity*) in the energetic neighborhood of the d^9 satellite. In such a case, we would not wish to include these d^{10} lines in our average, as this would imply that the satellite were not pure d^9. One way around this would be to eliminate from our average all lines below some cutoff intensity, say 2% of the intensity of the strongest line in the spectrum. In practice, such a distinction introduces only relatively minor differences in the theoretical final-state configuration. The reason is that all neighboring lines are sufficiently well hybridized so that the calculation using either method yields similar results.

In Fig. 4 we present the local d^8, d^9, and d^{10} configurations calculated according to Eq. (10), with the Ni $3p$ spin-integrated spectrum plotted on the same energy scale for convenient reference. We see that the leading edge of the main line is 80–90% d^{10}, and the trailing edge is roughly 70–80% d^{10}. Therefore, the nominally $d^9\ {}^3F$ lines get largely mixed into the nearby d^{10} states, leading to a strongly hybridized mixture of the two. Even so, as we have seen, analysis of the purely $d^9\ {}^3F$ term for the zero-bandwidth limit correctly explains the minority-spin polarization of the main line.

We also see from Fig. 4 that satellite B is roughly half d^9 and half d^{10}, while satellite C is roughly 60% d^9, 35% d^{10}, with a little d^8 mixed in. If we eliminate all lines below a 2% cutoff intensity, we find that the d^9 character of satellite B is increased by 10–15%, and the d^9 character of satellite C is increased by 15–20%.

Finally, we observe that most of the d^8 states occur 20–25 eV to the left of the main line. These states are not excited in our model due to the absence of d^8 in our ground state.

IV. CONCLUSIONS

We have presented theoretical Ni $3p$ photoemission spectra calculated within a periodic small-cluster model. Theoretical results were found to compare very favorably with experimental spin-resolved spectra. We examined theoretical spectra for a variety of limiting cases, thereby gaining considerable physical insight into the underlying structure. We showed that, upon introduction of a valence bandwidth, there is a strong transfer of spectral weight to the main line. We showed further that this spectral weight transfer depends on the ratio of the valence bandwidth to the effective Hubbard interaction U_{eff}. Finally, we discussed hybridization effects and configuration mixing in the final state, and calculated the local atomic configuration as a function of binding energy.

ACKNOWLEDGMENTS

The author gratefully acknowledges L. M. Falicov, who inspired the work. The author is also grateful to C. S. Fadley for general support throughout the final stages of the work, and to L. E. Klebanoff for stimulating discussions and use of experimental data. The helpful suggestions of Lisa Borland are especially appreciated. This work was supported in part by the Director, Office of Energy Research, Office of Basic Energy Sciences, Materials Sciences Division of the U.S. Department of Energy under Contract No. DE-AC03-76SF00098. J. G. Menchero also gratefully acknowledges support during this period from the Dean's Office of U.C. Berkeley.

[1] F. U. Hillebrecht, R. Jungblut, and E. Kisker, Phys. Rev. Lett. **65**, 2450 (1990).
[2] Y. Liu, Z. Xu, P. D. Johnson, and G. van der Laan, Phys. Rev. B **52**, R8593 (1995).
[3] D. G. Van Campen, R. J. Pouliot, and L. E. Klebanoff, Phys. Rev. B **48**, 17 533 (1993).
[4] L. E. Klebanoff, D. G. Van Campen, and R. J. Pouliot, Phys. Rev. B **49**, 2047 (1994).
[5] A. K. See and L. E. Klebanoff, Phys. Rev. B **51**, 11 002 (1995).
[6] H. Ebert, L. Baumgarten, C. M. Schneider, and J. Kirschner, Phys. Rev. B **44**, 4406 (1991).
[7] G. Rossi, F. Sirotti, N. A. Cherepkov, F. Combet Farnoux, and G. Panaccione, Solid State Commun. **90**, 557 (1994).
[8] G. van der Laan and B. T. Thole, J. Phys. Condens. Matter **4**, 4181 (1991).
[9] R. H. Victora and L. M. Falicov, Phys. Rev. Lett. **55**, 1140 (1985).
[10] J. G. Menchero, Phys. Rev. Lett. **76**, 3208 (1996).
[11] J. G. Menchero, Phys. Rev. B **55**, 5505 (1997).
[12] C. S. Wang and J. Callaway, Phys. Rev. B **15**, 298 (1977).
[13] S. M. Goldberg, C. S. Fadley, and S. Kono, J. Electron Spectrosc. Relat. Phenom. **21**, 285 (1981).
[14] N. A. Cherepkov, J. Phys. B **12**, 1279 (1979).